AFRL-AFOSR-UK-TR-2022-0044

Investigation of the properties of imploding plasma and the magnetic-field distribution using a novel spectroscopic technique

Maron, Yitzhak
Weizmann Institute of Science
234 Herzl
REHOVOT, , 00761000
IL

05/17/2022
Final Technical Report

Air Force Research Laboratory
Air Force Office of Scientific Research
European Office of Aerospace Research and Development
Unit 4515 Box 14, APO AE 09421

REPORT DOCUMENTATION PAGE

PLEASE DO NOT RETURN YOUR FORM TO THE ABOVE ORGANIZATION.

1. REPORT DATE	2. REPORT TYPE	3. DATES COVERED	
20220517	Final	START DATE 20170115	END DATE 20220114

4. TITLE AND SUBTITLE
Investigation of the properties of imploding plasma and the magnetic-field distribution using a novel spectroscopic technique

5a. CONTRACT NUMBER	5b. GRANT NUMBER	5c. PROGRAM ELEMENT NUMBER
	FA9550-17-1-0097	61102F
5d. PROJECT NUMBER	**5e. TASK NUMBER**	**5f. WORK UNIT NUMBER**

6. AUTHOR(S)
Yitzhak Maron

7. PERFORMING ORGANIZATION NAME(S) AND ADDRESS(ES)
Weizmann Institute of Science
234 Herzl
REHOVOT 00761000
IL

8. PERFORMING ORGANIZATION REPORT NUMBER

9. SPONSORING/MONITORING AGENCY NAME(S) AND ADDRESS(ES)	10. SPONSOR/MONITOR'S ACRONYM(S)	11. SPONSOR/MONITOR'S REPORT NUMBER(S)
EOARD UNIT 4515 APO AE 09421-4515	AFRL/AFOSR IOE	AFRL-AFOSR-UK-TR-2022-0044

12. DISTRIBUTION/AVAILABILITY STATEMENT
A Distribution Unlimited: PB Public Release

13. SUPPLEMENTARY NOTES

14. ABSTRACT
Under this Grant, Prof Yitzhak Maron and his team at Weizmann Institute performed small scale Z-pinch experiments. A Z-pinch uses a high current plasma discharge in a diode configuration with a gas puff in between to generate extremely high magnetic fields (B) to compress and heat up ions in a gas. The typical application of a Z-pinch is inertial confinement fusion of deuterium or lithium to generate neutrons. Using detailed spectroscopic measurements, highly resolved in both time and space, a self-generated plasma rotation, with Dr. Finch, Princeton University, and Dr. Velikovich, Naval Research Laboratory, they demonstrated using a cylindrical implosion with a pre-embedded axial magnetic field (Bz0). The rotation direction was found to depend on the direction of Bz0 and its' velocity is found comparable to the peak implosion velocity, considerably affecting the force and energy balance throughout the implosion. Moreover, the evolution of the rotation is consistent with magnetic flux surface iso-rotation, a novel observation in a Z pinch, which is a prototypical time dependent system. The diagnostic methods developed by University of Weizmann include two methods: the first method used a chordal Laser-Induced-Fluorescence (LIF), where the plasma density distribution in the r – Î¸ plane, is obtained with ~1 millimeter resolution in a single measurement. The second plasma diagnostic method used chordal interferometry, where Abel inversion of the data gives the radial density distribution. Here, U. Weizmann obtained the density distribution for each axial location to improve the measurement accuracy. The use of the two methods simultaneously turned out to be uniquely important for substantiating the measurement reliability, and for obtaining an absolute calibration for the LIF method. In addition, Prof Maron and his team developed non-linear Stark and Zeeman diagnostic methods and analysis routines to measure the electric and magnetic fields within the Z-Pinch. The primary purpose of the diagnostics was to achieve a detailed study of the physics going on in a Z-pinch. In addition, the diagnostics data providing highly detailed data, which could be used to verify highly complex Z-pinch fusion and other plasma discharge models. In addition, spectroscopic measurements of azimuthal magnetic field that only part of the driver current is flowing within imploding plasma radius when preembedded axial magnetic field (Bz0) is present. It was shown that when Bz0 = 0.4 T, low-density plasma (LDP) region exists at large radii, surrounding main imploding argon plasma. Substantially higher electron temperature (Te) and density (ne) in the presence of Bz0, indicate that part of the current flow in this region. To quantify how much of the driving current flows through the LDP, dedicated B-field measurements in the LDP region were conducted.

15. SUBJECT TERMS

16. SECURITY CLASSIFICATION OF:			17. LIMITATION OF ABSTRACT	18. NUMBER OF PAGES
a. REPORT U	b. ABSTRACT U	c. THIS PAGE U	SAR	25

19a. NAME OF RESPONSIBLE PERSON	19b. PHONE NUMBER *(Include area code)*
NATHANIEL LOCKWOOD	314-235-6005

Weizmann Institute of Science
76100 Rehovot, Israel
The Physics Faculty,
Phone +972 8 934 4055
Fax: +972 8 934 4172
Professor Yitzhak Maron
The Stephen and Mary Meadow
Professorial Chair
of Laser Photochemistry
Plasma Laboratory, Head

March 30, 2022

Final Report for United States Air Force – Office of Scientific Research

PI: Prof. Yitzhak Maron

Table of Contents

Spectroscopic magnetic field measurements of gas-puff Z-pinch

Determination of Gas Valve density and flow by Laser-Induced-Fluorescence and laser-interferometry

The gas valve was mounted on the Z-pinch generator and tested against various gas pressures and voltage settings. The operating pressure was chosen to be 20 psi and the target gas was chosen as O_2 from considerations of spectroscopic diagnostics. The optimal operating voltage for the valve was measured to be ~600 volts for the chosen pressure. Two diagnostic systems were developed for measuring the time-dependent 2-dimensional density distribution of a cylindrical gas jet injected into vacuum through a valve-nozzle system. The first method used is chordal Laser-Induced-Fluorescence (LIF), where the density distribution in the $r - \theta$ plane, is obtained with ~1 millimeter resolution in a single measurement. In this method, the gas is doped with a tracer, which fluoresces due to excitation by a laser beam. The laser beam is made to be cylindrical, with a diameter of 1mm in the desired z-position, through the center of the cylindrical puff. The fluorescence is captured with either a regular or an intensified 2-dimensional Charge-Coupled-Device (CCD) camera. In figure 1, the results of such chordal LIF measurements are presented. The measurement is made of 9 separate shots of the valve, in the corresponding axial position, across the 9 mm AK gap. The second method used is chordal interferometry, where Abel inversion of the data gives the radial density distribution. Here, numerous measurements are made to obtain the density distribution for each axial location and to improve the measurement accuracy. The use of the two methods simultaneously turned out to be uniquely important for substantiating the measurement reliability, and for obtaining an absolute calibration for the LIF method. Extensive examinations were made to assess and to reduce the uncertainties for the two methods, which allowed for obtaining detailed 3-dimensional information of the gas density distribution and flow. Results of these

measurements served for the design of a novel triple-valve-nozzle concept [1]. In this system, different pressures can be used in each plenum. The uniformity, and the deviations from uniformity, have been investigated on a mm spatial scale. Also studied is the combination of valve pressures required to tailor a specific density distribution. We note that such detailed measurements are highly useful in providing the initial conditions required for the simulations of the plasma-dynamics in various experiments, as has been well demonstrated in the simulations of our Z-pinch experiment by our colleagues at NRL [2].

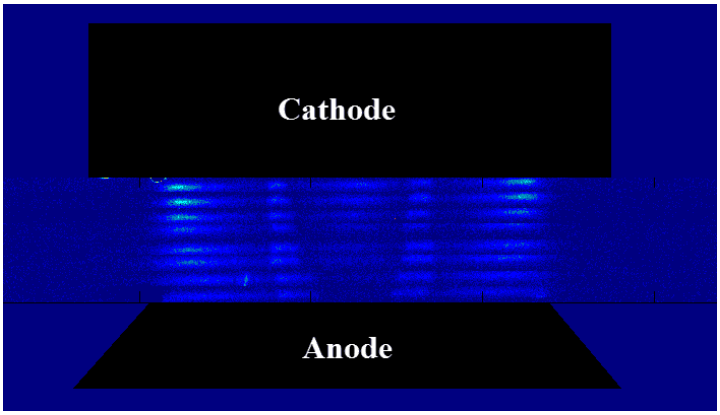

Figure 1: LIF measurements of our cylindrical puff-on-jet z-pinch nozzle. Intensity is arbitrary.

Experimental setup

The lumped circuit model of the z-pinch generator is composed of a capacitor bank (5.5 μF), charged to 60 kV, in series with a resistor (20 mΩ), an inductor (30 nH), and the gas-puff load with an initial inductance of 1.160.5 nH. The generator drives a peak current of 500 kA, rising in 500 ns as measured by a calibrated $\dot{B}$ probe. The oxygen gas-puff is injected through a double nozzle composed of a central opening of diameter 2.6mm and an outer annular opening spanning 34.4‑38mm in diameter. The nozzle exit plane is recessed by 4mm from the edge of an annular sleeve serving as the cathode. The anode wire mesh is also housed in an annular sleeve and is set back 5 mm from the edge of the annulus. There is a 9 mm gap between the cathode edge and the anode edge. The oxygen gas-puff consists of an on-axis jet, ~5 mm in diameter, surrounded by a thick shell. Due to the radial expansion of the shell along the flow toward the anode, the shell is initially conical with an outer diameter of ~40 mm at the nozzle, which extends to nearly 60 mm close to the anode

(see Fig.1 and Fig. 3(a) in [3]). Stagnation on axis is reached in ~500 ns and lasts ~10 ns, during which x-rays are emitted.

Spectroscopic measurements

The spectroscopic measurements were made using an optical-fiber linear-to-linear array, consisting of a single row of 50 fibers, each is 200 μm in diameter and 4.05 m in length. Each of the arrays can be oriented either to view several z-positions at a single y-position, or to view several chords at a single z-position. In previous studies, X-ray spectroscopy of our neon plasma produced from the puff-on-puff system, showed that the electron temperature at stagnation exceeds 200 eV [4] [5]. During this time, He-like, H-like, and bare-nuclei ions exist within r ~ 0.5 mm. Visible-light images of the same plasma revealed intense radiation emitted 15 ns before stagnation from radii of up to r ~ 2 mm [6].

These measurements indicated that lower ionization levels, in particular Li-like (Ne VIII), prevail at radii that are between 1 mm and 5 mm. To avoid the continuum from the stagnating plasma we used chordal views with y > 1 mm and end-on views for r > 1 mm. An example of the calculated shapes of the Ne VIII 3s-3p transitions with and without magnetic field (with a rather broad distribution) is given in Fig. 1. As explained in the caption, the presence of a magnetic field cannot be inferred from the shapes of each of the components separately, given for comparison in the inset (A). Indeed, the $^2S_{1/2}$–$^2P_{3/2}$ component does not exhibit any feature of the Zeeman effect (the extra broadening might be also caused by a higher electron density or a strong turbulence), while the shape of the $^2S_{1/2}$–$^2P_{1/2}$ component might be explained by the Doppler effect or by self-absorption of the light by the colder outer layers of the pinch. Thus, it is only the simultaneous observation of the two components that can rule out these possibilities and provide unambiguous detection of the magnetic field in the plasma (see Refs. [7] [8]).

Results of experiments made with O_2 gas are presented in Figs. 1 to 3. Although at late times radial (y = 0) measurements show only continuum radiation, O VI lines are clearly seen at y-positions a little farther from 0. Spectral lines of various charge states, beneficial for the determination of the plasma properties, are well observed up to y ~10 mm from the z-axis.

Fig. 3 shows a few spectra obtained from Fig. 2, the analysis of which is expected to provide a wealth of information. Fig. 4 shows the visible imaging corresponding to Fig. 2. It allows determining that for z = 8 mm (where the spectra of Fig. 2 were taken), the plasma column is the narrowest and is relatively uniform.

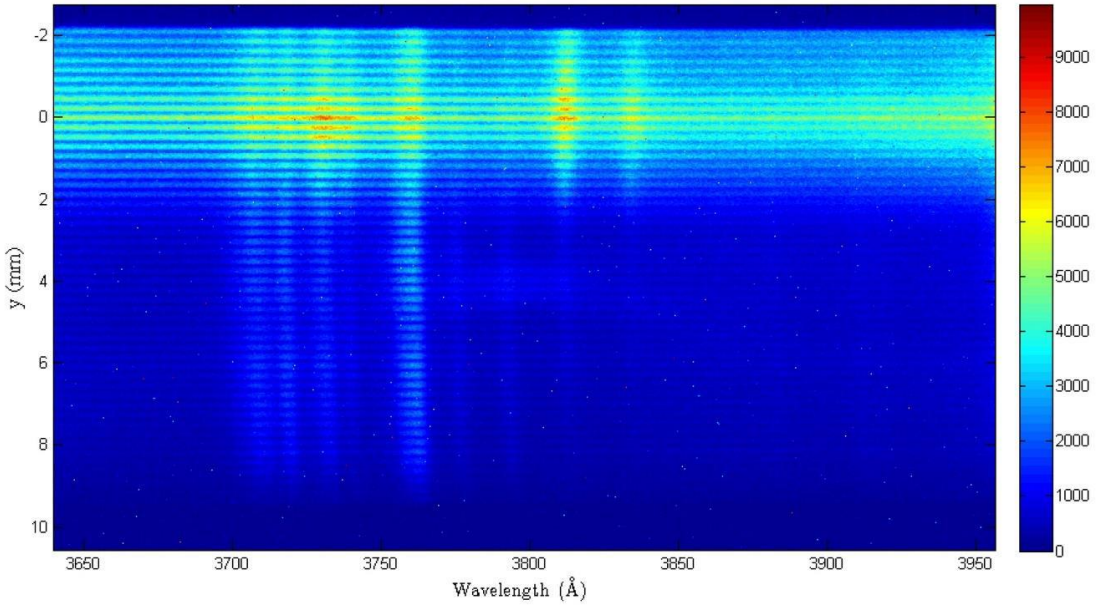

Fig. 2: Oxygen spectra recorded by the 30-cm spectrometer using the 1200 grooves per mm grating, 9 ns before stagnation, with a 10-ns exposure. Here, 50 fibers are aligned linearly, viewing the plasma at z = 8 mm from the cathode for $-2mm<y<10mm$. Intense continuum radiation from the stagnating plasma can be seen at y=0 (a view along the diameter), while several spectral lines are observed for all distances from the axis viewed.

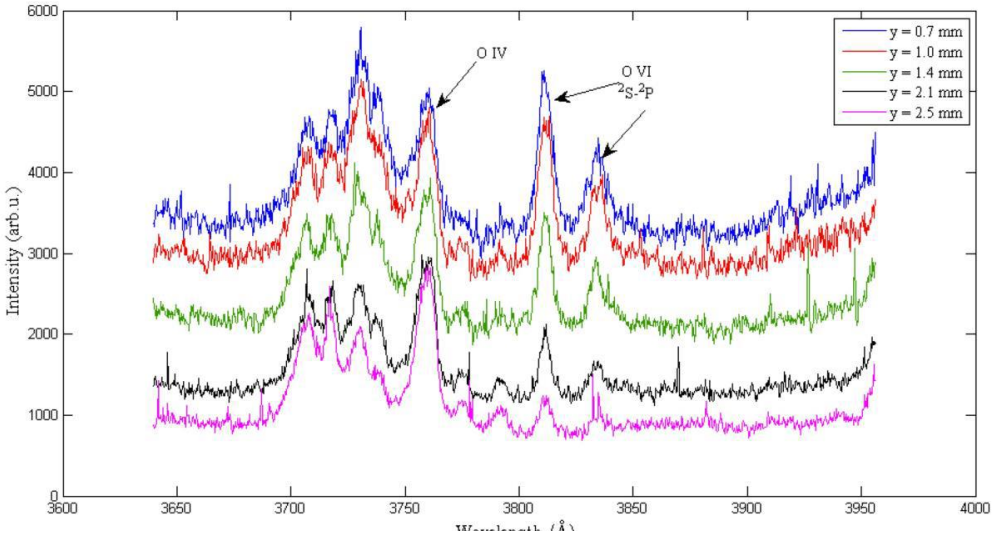

Fig. 3: Spectra obtained by a few fibers selected out of the 50 fibers seen in Fig. 2.

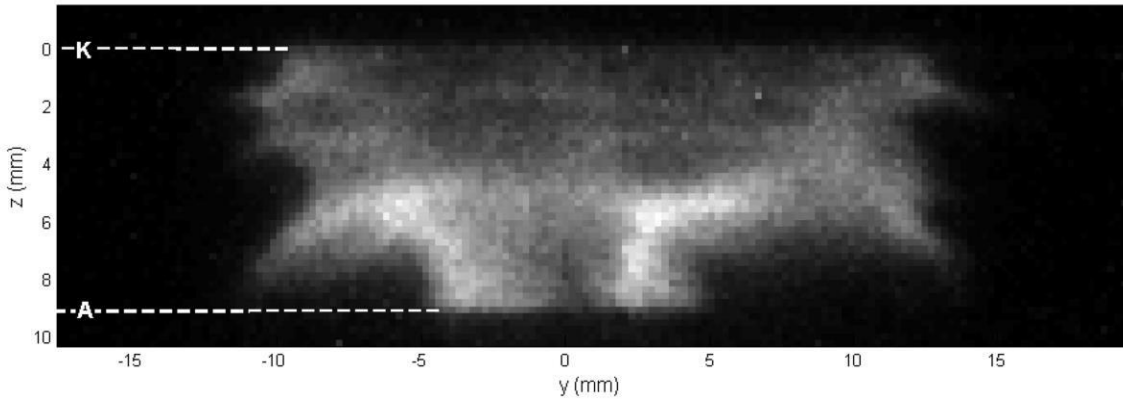

Fig. 4: 2-dimensional side-on image of the oxygen plasma at the time of the spectra given in Fig. 2, with a 10-ns exposure.

The diagnostic method – polarization spectroscopy

The diagnostic method is thoroughly described in Ref. [3]. In short, when the perturbation in the energy levels due to the magnetic field is small compared to the fine-structure energy separations, the magnetic-field-induced splitting for both the upper and lower levels of the transition is given by $\Delta E = g_{LSJ}\mu_B M B$, where B is the magnitude of the magnetic field $\vec{B}$, M is the projection of the total angular momentum J of the given state in the direction of $\vec{B}$, μB is the Bohr magneton, and g_{LSJ} is the Landé g factor [7]. If a dominant direction of $\vec{B}$ exists, the emissions from the components of a Zeeman split transition are polarized. When the emission is viewed parallel to $\vec{B}$, only its σ components are visible, and the light is circularly polarized, right handed for $\sigma+$ ($\Delta M=+1$) and left handed for $\sigma-$ ($\Delta M=-1$). Discriminating between the $\sigma+$ and $\sigma-$ components, observed along multiple chords through the plasma, is achieved by means of a quarter-wave plate and a polarizing beam splitter. The radiation is split into two beams, each carrying one of the now orthogonal linear polarizations, and directs each beam to a different branch of a bifurcated optical fiber array. The joint end of the array is imaged onto the entrance slit of a 1.26-m spectrometer equipped with a 2400 grooves/mm grating. The spectra of both polarizations are recorded simultaneously using an intensified charge-coupled-device (ICCD) camera coupled to the

exit focal plane of the spectrometer. While the $\sigma+$ components are always blue-shifted with respect to the unpolarized emission line, the $\sigma-$ components are always redshifted. This method therefore relies on the line positions rather than on their shapes and is thus applicable even when the lines are Stark and Doppler-dominated and is nearly unaffected by opacity.

The diagnostic method can only be used with lines of sight that are parallel to $\vec{B}$. This appears to yield only a single data-point per experiment, which provides B at the outermost radius of the plasma column. Using Ampère's law, this data-point provides only the total current flowing through the plasma. In contrast, in this work, we overcame this limitation and were able to penetrate the plasma column and directly determine the magnetic field radial distribution. We accomplished this by taking advantage of the naturally occurring charge-state radial distribution and recording spectral lines emitted from different charge states simultaneously. In both low- and high-current Z-pinch experiments producing a high K-shell emission yield, only ~15% of the imploding plasma is heated at stagnation to conditions necessary to radiate K emission [4,9] . This generates a considerable temperature gradient dropping from the hot core toward the peripheral plasma, which in turn generates a radial charge-state distribution, from highly charged ions found at the core to lower charge states that reside at outer layers (as illustrated in Fig. 2 of [3]). Therefore, the field radial distribution can be measured by observing the Zeeman effect from emissions of several charge states simultaneously, each emitted from the outermost radius for which a satisfactory signal is obtained.

Results of spectroscopic measurements

Eight magnetic field radial distributions [3], measured at eight moments in time at three different axial positions are presented in Figs. 5-7. We note that each distribution was obtained from a separate discharge. The field value at the innermost radial position is obtained from the Zeeman splitting of the O VI line. At the next radial position, the value is obtained from the O III line. The error bars for these data-points were derived from the accuracy in which the emission wavelengths could be determined. In some cases, the SNR was such that a range of Voigt profiles could be fit, thus increasing the uncertainty. To this, the contribution of the systematic error discussed above were incorporated. The outermost

radial position of the O III ions was used for the middle radial position. R_0 was measured from 2D plasma imaging. The magnetic field value was measured using the Zeeman splitting of the Oxygen ions (O III and O VI for the innermost and middle radial positions, respectively. The magnetic field value at R_0 is the boundary magnetic field, B_0 and is obtained via Ampère's law, namely:

$$B_0 = \frac{2I_0}{R_0 c} \tag{1}$$

where I_0 is the entire circuit current measured by the $\dot{B}$ probe outside the pinch region and c is the speed of light. The agreement between the two methods of calculating B at the plasma edge in this shot proves that the entire circuit current flows within the outer radius of the visible plasma cylinder. Therefore, B_0 was calculated for each discharge and added to each distribution.

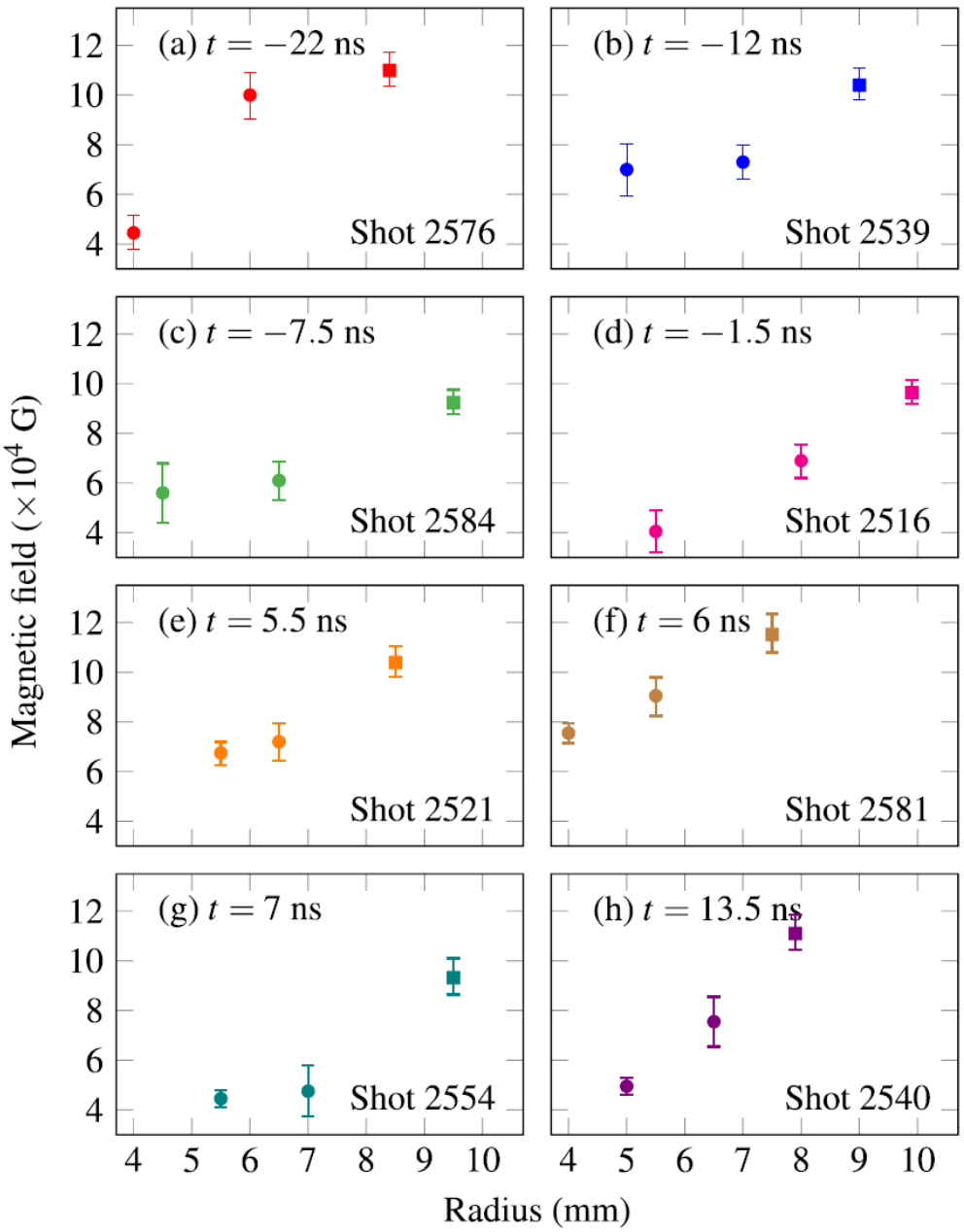

Fig.5 – Magnetic field distributions at eight moments in time and z = 2 mm. The circles represent values obtained from the O VI (innermost radii) and O III spectral lines, and the squares represent the boundary magnetic field, B_0, obtained from I_0, see text for details.

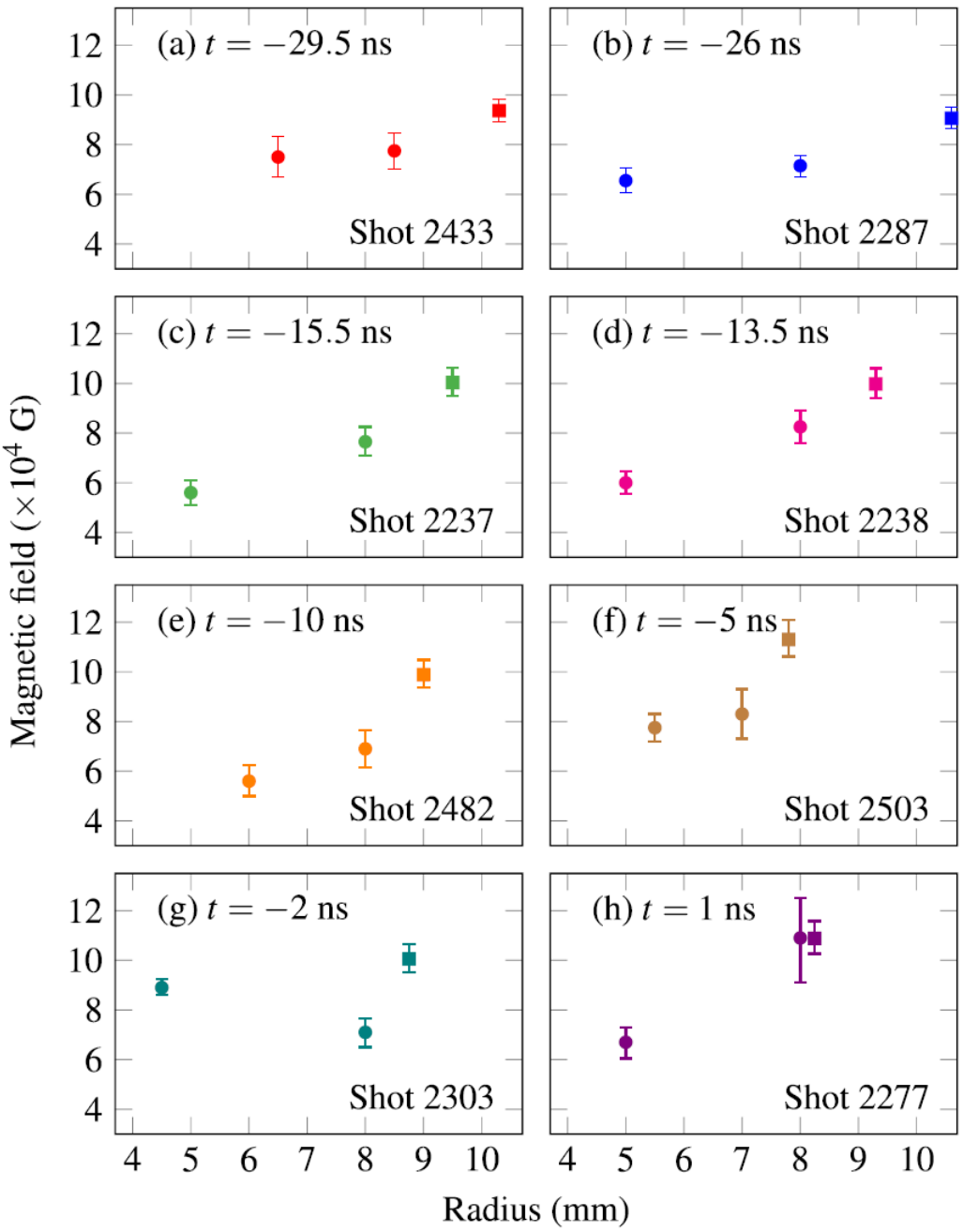

Fig.6 – Magnetic field distributions at eight moments in time and z = 5 mm. The circles represent values obtained from the O VI (innermost radii) and O III spectral lines, and the squares represent the boundary magnetic field, B_0, obtained from I_0. The distribution at t = 1 ns (shot 2277) shows that when the radial position of the O III line is almost R_0, the measured magnitude agrees with the value of B_0. This proves that indeed the entire circuit current flows within R_0 and validates the use of Eq. (1) for obtaining B_0.

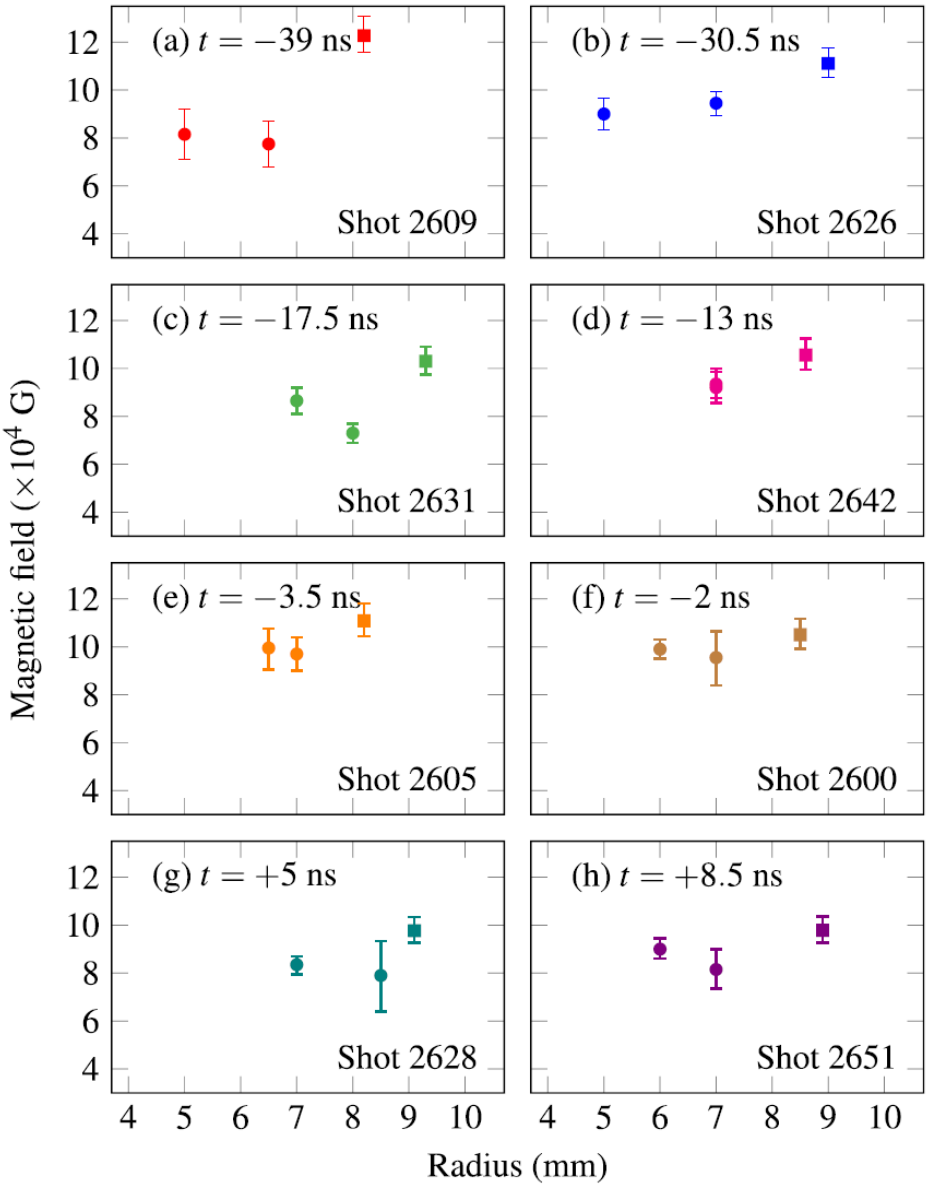

Fig.7 – Magnetic field distributions at eight moments in time and z = 8 mm. In (d), the O III and O VI data points overlap. This results from the fact that both charge states were found in the flaring arcs discussed in the text. While the two states cannot coexist and still emit detectable lines,13 for very thin flares, they may be too close to be discriminated by the spatial resolution of the diagnostic system. The fact that the independent analysis of both lines yielded the same field magnitude strengthens the validity of the method and the analysis.

Spectroscopic magnetic field measurements of gas-puff Z-pinch with preembedded axial magnetic field

Experimental setup

In the experiment a cylindrical configuration is used. A quasi-static, nearly uniform, axial magnetic field of up to 0.4 T is generated by a pair of Helmholtz coils (HC). Each coil has a radius of 50 mm and is driven by a slow circuit (rise time ≈ 5 ms) to allow the magnetic field to penetrate the anode-cathode gap through the conducting metal electrodes. When the initial axial magnetic field, B_{z0}, reaches its maximum, the gas load is injected into the 10-mm long anode-cathode gap by a fast gas-puff system with a de-Laval nozzle. The nozzle forms a hollow cylindrical gas shell with an external radius of 19 mm and internal radius of 7 mm. Argon gas was used and the discharge is initiated when the gas load per length reaches 30 μg/cm. The current pulse is generated by simultaneously discharging 4 high voltage 4-μF capacitors connected in parallel, driving a 300-kA current pulse with a rise time of 1.6 μs. The high-voltage pulse results in a gas breakdown and the produced plasma carries a current that exerts J×B force in the inward radial direction, compressing the gas together with the pre-embedded axial magnetic field.

Visible-UV spectroscopic systems, depicted in Fig. 8a, are used to study the LDP composition and electron temperature (T_e) and density (n_e) and the current distribution. In one system, used to determine the plasma parameters, the radiation emitted from the plasma is imaged on the entrance slit of a 0.5-m imaging spectrometer, using a spherical mirror (f = 0.6 m). A gated (3 ns) ICCD camera is attached to the spectrometer's exit slit plane. The instrumental profile is close to a Gaussian with FWHM of ~0.7 Å (for a grating of 1200 groves/mm and entrance slit of 60 μm). The observed plasma cross section at the focal plane is 90- μm along z and 26 mm in the radial direction, with spatial resolution of ~ 300 μm.

Study of the current distribution in the plasmas is performed by simultaneous measurements of B_θ in the main imploding plasma and in the LDP region. This is achieved by using two identical spectroscopic systems and employing a polarization technique for

discriminating between the left- (σ^-) and right-handed (σ^+) circularly polarized Zeeman emissions, described in previous chapter and references [3,10,11].

Spectroscopic measurements of periphery plasma region of Z-pinch with pre-embedded axial magnetic field applied

In reference [11], it was shown from spectroscopic measurements of azimuthal magnetic field that only part of the driver current is flowing within imploding plasma radius when pre-embedded axial magnetic field (B_{z0}) is present. It was shown that when B_{z0} = 0.4 T, low-density-plasma (LDP) region exists at large radii, surrounding main imploding argon plasma. Substantially higher electron temperature (T_e) and density (n_e) in the presence of B_{z0}, indicate that part of the current flow in this region. To quantify how much of the driving current flows through the LDP, dedicated B_θ measurement in the LDP region were conducted.

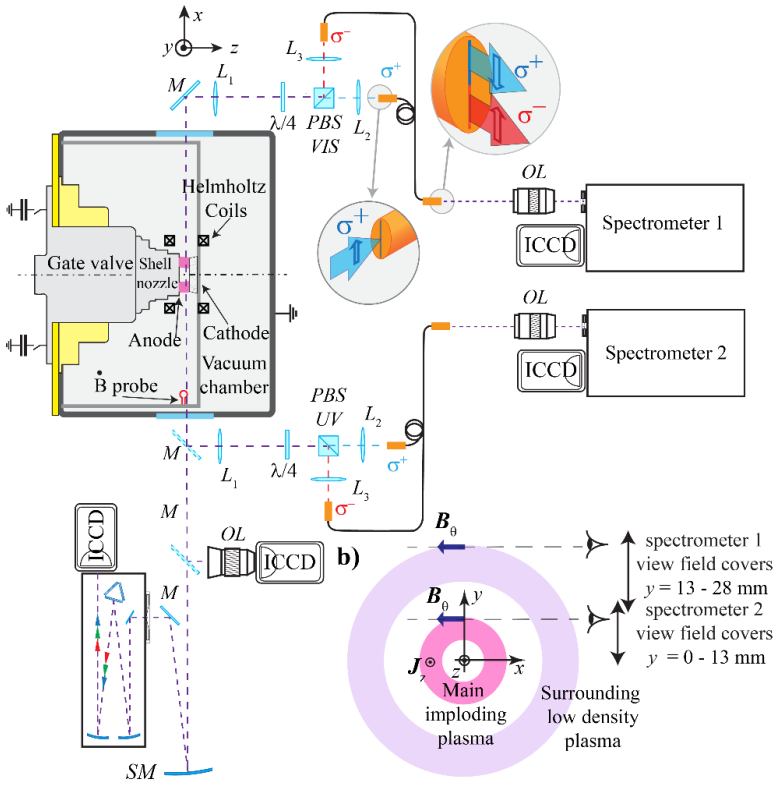

Figure 8. a) The schematics description of the experimental setup and spectroscopic system used for B_θ measurements. PBS stands for polarizing beam splitter, L_1, f_{L1} = 200 mm, L_2=L_3, f_{L2} = 150 mm lenses, M – mirror, SM, f_{SM} = 600 mm, spherical mirror, λ/4 – quarter wave plate, OL – objective lens. b) Line of sight of spectrometer 1 observing LDP emission in y-direction from 13 to 28 mm and spectrometer 2 observing emission of argon imploding plasma in y-direction from 0 to 13 mm.

Measurements of azimuthal magnetic field

The procedure of B_θ determination is described in previous chapter and publications [3,10,11]. The same procedure is used to determine B_θ using C IV transition 3*s* - 3*p* at λ_0 = 5801.33 Å. Typical examples of spectral recording of σ^+ and σ^- Zeeman component C IV line at λ_0 = 5801.33 Å are shown in Fig 9.a,b. The dashed white vertical line in Fig.9, shows the wavelength position in the absence of *B*-field, demonstrating the Zeeman-induced wavelength shift of the two σ-Zeeman components. Figs.9c and d show the experimental line shapes of the σ^+ (blue circles) and σ^- (red diamonds) Zeeman components, along with their best fits (blue solid line and red dashed line). The line shapes are obtained from the spectral image Fig 9a, b) by averaging over $\Delta y \sim 1.5$ mm in the radial

direction (*y*-coordinate) at the outer radius of the C IV line in the LDP (between ~24.5 mm and ~27 mm), marked with red and blue horizontal lines in Fig.9a, b. The outer radius of the C IV in the LDP is defined at ~ 20-30 % of the peak intensity of the C IV line. Each of the σ^+ and σ^- line shapes are fitted with a Voigt profile, where the Gaussian part accounts for both the instrumental and Doppler broadening, and the Lorentzian part is due to the Stark broadening. B_θ is then extracted from the wavelength separation between the peaks of the best fits, by dividing it with 0.36 Å/T.

Results of systematic B_θ measurements at different times during the implosions and at different *z*-position, are shown in Fig.10 as red full circles. They show the time evolution of B_θ in the LDP region (lower row of graphs) together with the evolution of B_θ in the main imploding plasma (upper row of graphs) for B_{z0} = 0.4 T, at different *z*-positions. The right axis of the lower row of graphs in Fig.10 shows $r_{LDP}^{C\ IV}$ - the radius where B_θ in the LDP is measured. The right axis of the upper row of graphs in Fig.10 shows the outer radii of Ar III line in the main imploding plasma (which is the same as the outer radii of the main imploding plasma, as confirmed by filtered visible imaging) - the radius where B_θ in the main imploding plasma is measured. Based on Ampere's law, the calculated values of B_θ, obtained by using the measured total current and the outer radii of the main argon plasma (upper row of graphs) or the outer radii of the LDP (lower row of graphs), are shown as blue triangles in graphs in Fig.3. The difference between the calculated and the measured values of B_θ seen in the upper row of graphs in Fig.3 is significant, much larger than the error bars, and it is visible at all *z*-positions along A-K gap. These results show that large part of the driving current is not flowing within the main imploding argon plasma. The difference is increasing along *z*-axis. The agreement between the calculated and measured values of B_θ for the LDP our radius (lower graphs in Fig.3) is generally good**,** showing that a large part of the driving current is flowing in the LDP region for B_{z0} = 0.4 T and that almost all of the driving current is accounted to flow within the radius $r_{LDP}^{C\ IV}$.

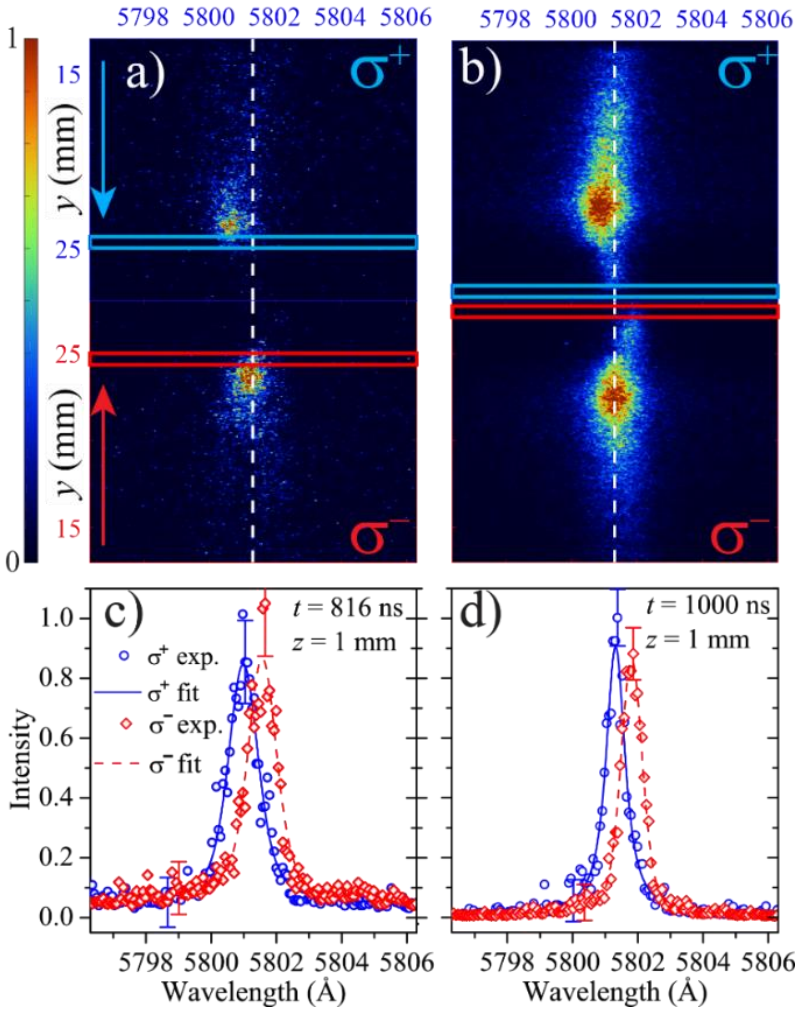

Figure 9. Spectral images of C IV transition $3s^2S_{1/2}$ - $3p^2P_{3/2}$ at λ_0 = 5801.33 Å used for B_θ measurements in the low density plasma for B_{z0} = 0.4 T at: a) t = 816 ns, z = 1 mm; b) t = 1000 ns, z = 1 mm. c) Spectral line shapes of the σ^+ (blue circles) and σ^- (red diamonds) Zeeman components along with the best fits (blue solid and red dashed lines) taken from a) at r = 24.5 mm. Measured B_θ = 1.5 T and $n_e = 10^{17}$ cm^{-3}. d) Same as in (c) where spectral line shapes are taken from (b) at r = 27 mm with measured B_θ = 1.4 T and $n_e = 8 \cdot 10^{16}$ cm^{-3}. The dashed white vertical line in (a) and (b) represents un-shifted position of the line center (B_θ= 0). The horizontal lines mark the line-out positions of (c) and (d).

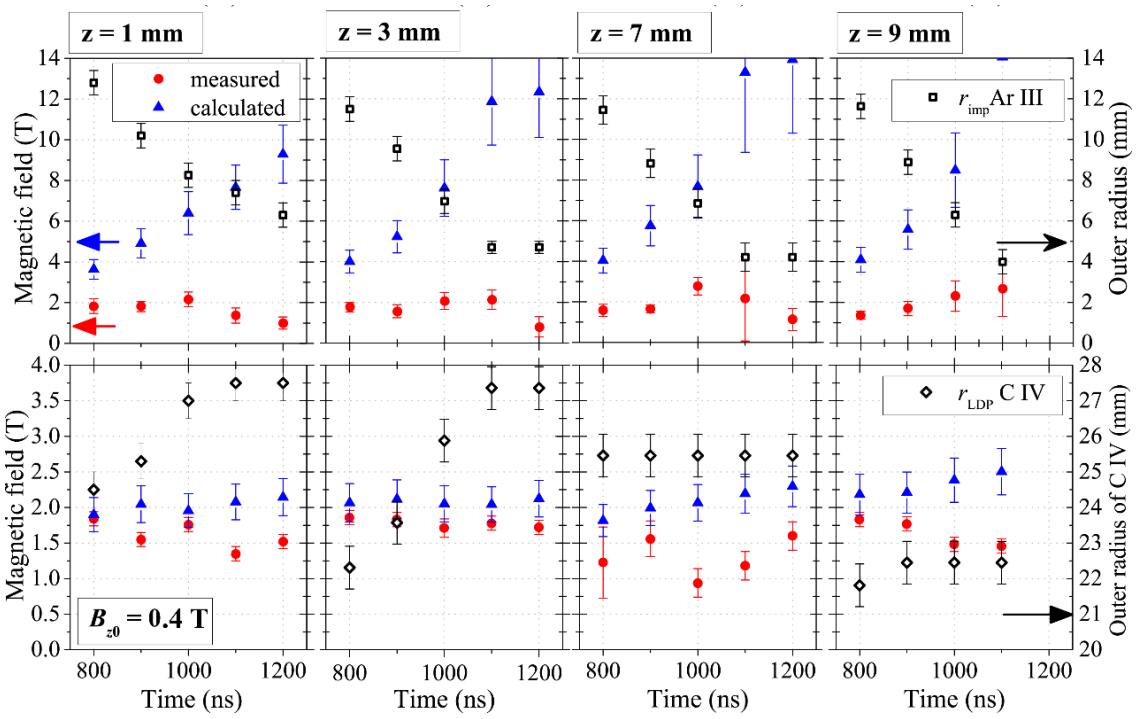

Figure 10. Time evolution of B_θ in the main imploding plasma (upper row of graphs) and in the LDP (lower row of graphs) at different z-positions along A-K gap. Measured B_θ values (red circles) are at outer radius of main imploding plasma (black open squares) or at outer radius of C IV line emission in the LDP (black open diamonds). Calculated B_θ values (blue triangles) are obtained from the total current and the outer radius of Ar III in the main imploding plasma or C IV in the LDP. Right axis denotes outer radius of the main imploding plasma in upper graphs, and outer radius of C IV line in the LDP in lower graphs, at which B_θ is measured.

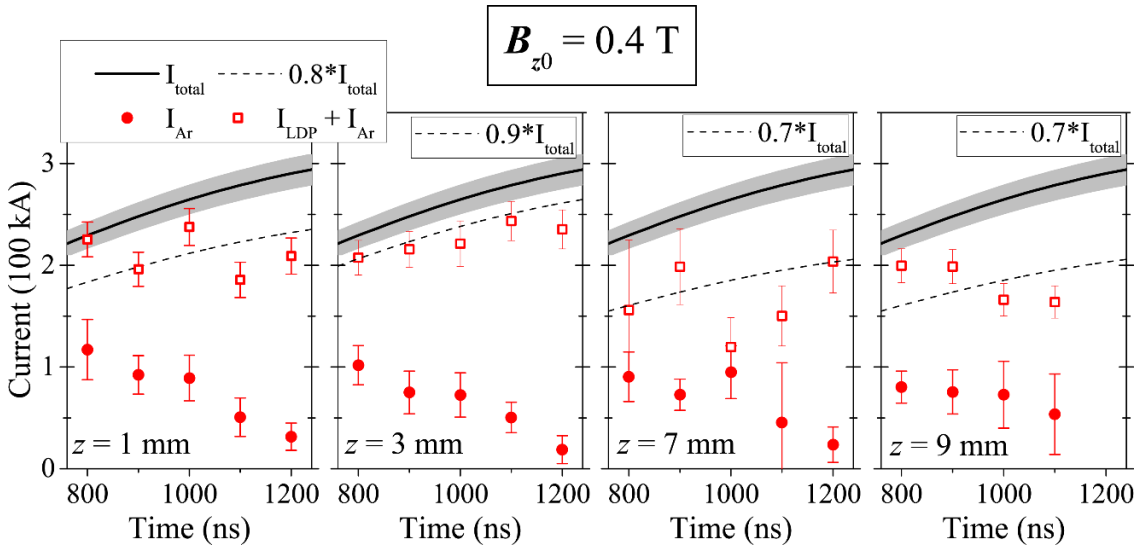

Figure 11. Evolution of current flow along z-positons. The graphs are obtained using data from Fig.3. representing them in the form of current that flows within measured radius. Black line represent typical current trace for B_{z0} = 0.4 T.

For z = 1 mm and z = 3 mm almost all current is accounted within the outer radius of C IV in the LDP. Discrepancies that exist at late times (>1000 ns) and at z=7 and 9 mm show that a small part of the current flows through even a lower-emission, lower-density plasma (n_e ~10^{15} cm^{-3}) at higher radii than the outer radii of C IV (r > 27 mm). Spatially resolved spectroscopic measurements along y-direction, up to y = 36 mm, actually show that hydrogen H_α line emission exists at radii higher than the outer radii of C IV in the LDP at all z-positions, indicating the possibility that this small missing part of the current is flowing at these large radii. The outer radius of hydrogen line in the LDP is unknown, since it surpasses r = 36 mm, which was the maxim radii of spectroscopic system that observes LDP.

Optical setup for measurements of plasma rotation in low-density-plasma region of Z-pinch with pre-embedded axial magnetic field

In previous section, C IV transition $3s^2S_{1/2}$ - $3p^2P_{3/2}$ at λ_0 = 5801.33 Å, is used for B_θ measurements of the low-density plasma (LDP) for B_{z0} = 0.4 T. Both sigma Zeeman components of C IV spectral line had additional spectral shifts in the same direction with respect to unperturbed spectral line wavelength.

To investigate the nature of this spectral shift, direction of the pre-embedded axial magnetic field was changed by changing voltage polarity of Helmholtz coils. It was observed that the spectral shifts changed direction, see Figure 12. In this way it is also confirmed that the spectral shift sign depends on the sign of $B_{z0.}$

To test the hypothesis that the observed spectral shift is in fact a Doppler shift that comes from rotation (and not from some lateral movement of plasma cross-section) it was necessary to observe spectral lines from opposite azimuths ($r+$, $r-$) at the same axial location. If Doppler shifts at opposite azimuths at the same axial location have opposite signs, this is clear evidence of a plasma rotation. For this a new optical setup is developed, see Figure 12a.

The new optical setup, shown in Figure 13a, consists of a lens and a mapped bifurcated optical fiber array. The LDP is observed side-on. Opposite azimuths at the same axial position of LDP region are imaged to the separate branches of the fiber array by the biconvex lens, f = 300 mm, dia. 75 mm, as shown in Figure 6a. Each branch of the fiber array consists of 50 individual fibers (200 um core width, 20 um width cladding) tightly packed in a line, one next to the other. Fiber branches are aligned one on top of the other so that line of 50 fibers in one branch continues the line of 50 fibers from the other branch. Separation between fiber branches exist in order to avoid plasma emission from the main imploding plasma, which is at least one order more intense than plasma emission that comes from LDP. View field of fiber branch 1 is from -28mm to -8 mm, while the view field of fiber branch 2 is from 8mm to 28 mm in radial direction. Both branches merge to the common end, where a line of 100 fibers (50 from each branch) is imaged to the entrance slit of a high-resolution spectrometer coupled with ICCD camera. The spectrometer spectral resolution is ~0.25-Å, while spatial resolution is defined by the view field of an individual fiber, and it is ~0.3 mm.

Spectroscopic data on Figure 6b show previously mentioned C IV line originating from LDP region, recorded at different azimuths at the same axial position on the same ICCD sensor. Upper part of ICCD recording shows azimuths from -28 mm until -8 mm, while lower part of the recording shows azimuths from 8 until 28 mm, both at axial position z = 3 mm, where z = 0 is anode surface. Figure 13c shows spectral lineouts taken from the

area marked in Figure 13b. Red dots represent the experimental line profile of C IV 5801.33-Å line taken from a radius of ~18mm, while blue dots are for the line profile taken from ~ -18 mm. Experimental profiles were fitted with Voigt function. Separation between the fit peaks shows clearly that rotation of low-density plasma exists.

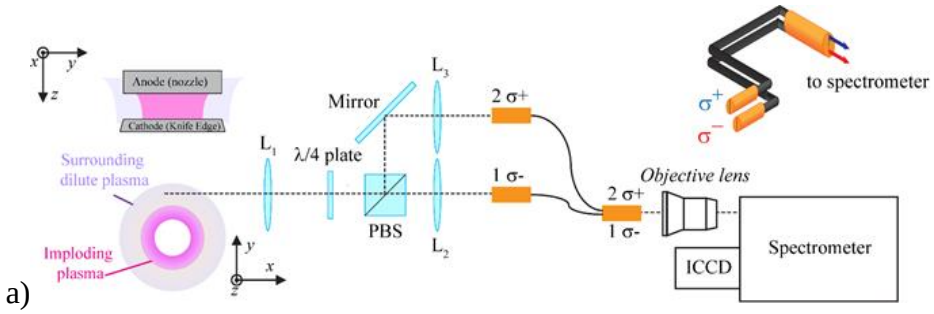

a)

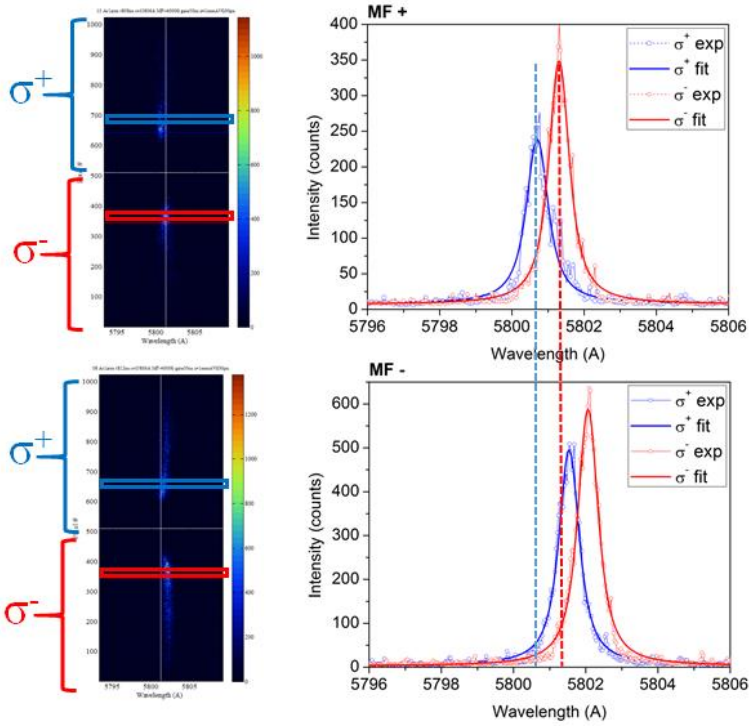

b)

Figure 12. a) Experimental setup used for measurements of B_θ in the low-density plasma (LDP) region of Z-pinch implosion with pre-embedded axial magnetic field, with the line of view to LDP. b) Example of spectral recordings of the σ+/σ- Zeeman components of CIV line with corresponding lineouts. Blue line corresponds to σ+ while red line corresponds to σ-. Upper part shows recordings when the pre-embedded axial magnetic field, B_{z0}, is in the positive direction (direction from anode (nozzle) to cathode). Lower part shows recordings when B_{z0} is in the negative direction. From comparison of upper and lower spectral lineouts it is obvious that spectral lines are shifted mutually.

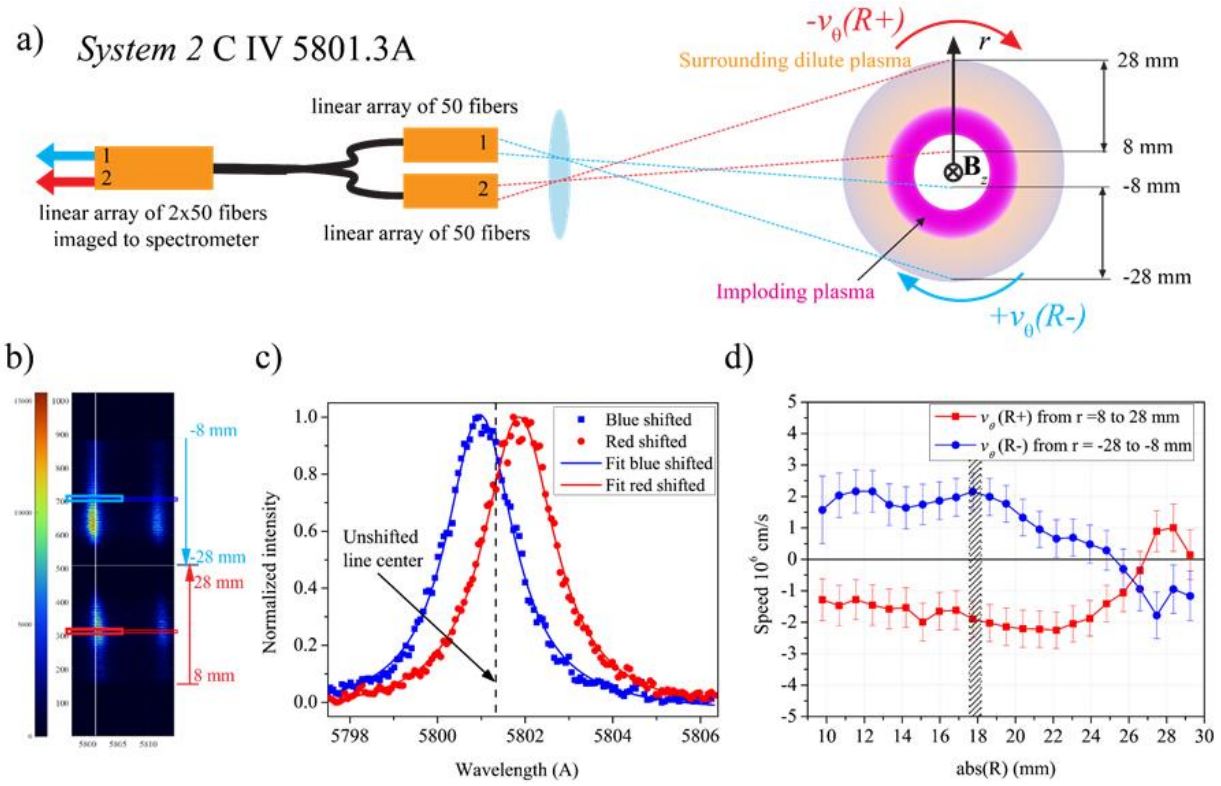

Figure 13. a) Simultaneous measurements $\Delta\lambda_{Doppler}(R)$ and $\Delta\lambda_{Doppler}(-R)$ in a single discharge with use of bifurcated optical fiber array. b) Spectral image of C IV 5801.3 A. Upper part of the image is plasma emission R [-28, -8] mm, lower part of the image is plasma emission R ~ (8,28) mm at the same z position. c) Spectra averaged over rectangles shown in b), R = 18 mm, ΔR = 0.6 mm is the area over averaging is done. d) Velocity of C IV ions over plasma radius.

Rotation of the low-density plasma (LDP) of Z-pinch implosion with pre-embedded axial magnetic field

Systematic measurements of Doppler shift of C IV line 5801.33-Å are done, in a way described in the previous section. By changing the delay time after current initiation and by recording spectra at different axial positions, spatially and temporally resolved rotation measurements of LDP are obtained and are shown in Figure 14. The spectral lineouts are taken at the low-density-plasma outer edge, which is *r*~ 22-26 mm, depending on the axial position. In this way, integration over the line of sight is avoided. Graphs in Figure 14 show the evolution of rotation speed of the LDP outer edge at different axial

positions, z = 1, 3, 5 and 7 mm. The red circles and black squares denote rotation velocities obtained from opposite azimuths. Time evolution is given from early time of discharge (~300 ns) until stagnation of the main argon plasma (~1180 ns).

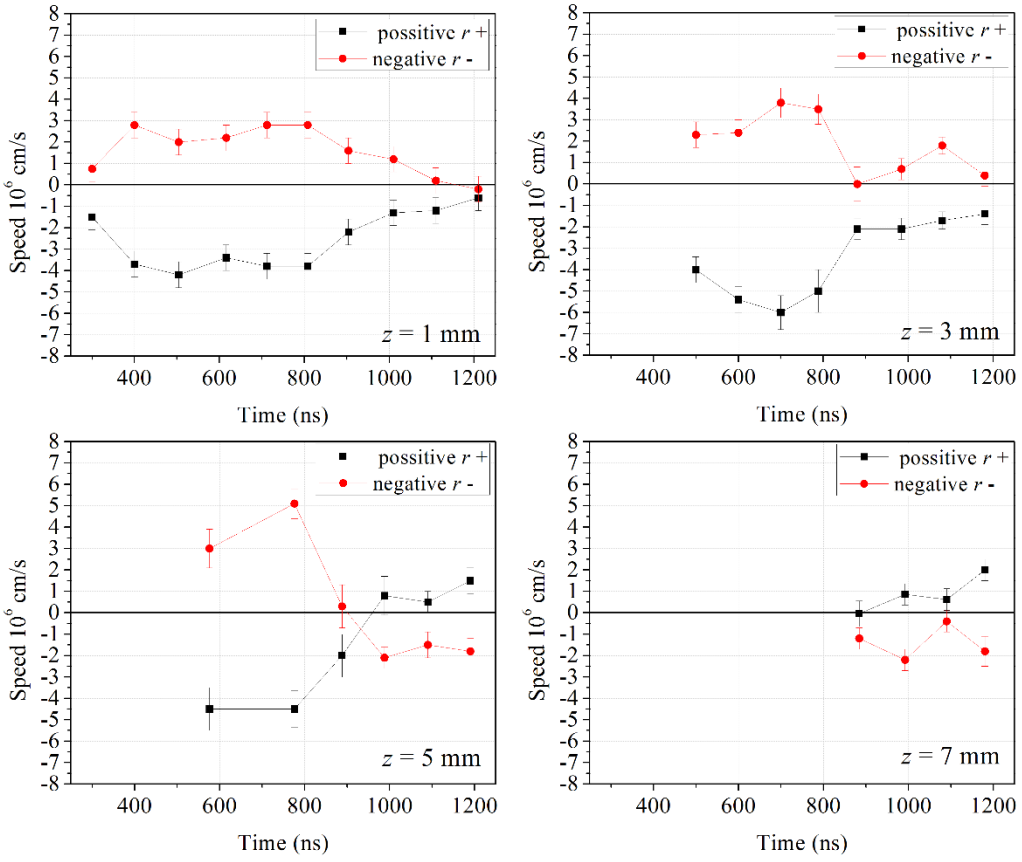

Figure 14. Time evolution of rotation speed of the LDP outer edge (r ~ 22 – 26 mm) at different axial positions, z = 1, 3, 5 and 7 mm.

Carbon impurity in LDP comes most probably as blow-off from nozzle (anode) and Helmholtz coils mounted near it. At z = 1 mm, due to the vicinity of nozzle, C IV 5801.33-Å line in LDP exist from early time (~300 ns) of implosion, and show significant rotation velocity which is kept almost constant up to ~900 ns on both azimuths. Velocity then decreases and disappears at ~1200 ns.

At z = 3 mm, emission of C IV 5801.33-Å line starts to appear later then at z = 1 mm, due to later time it arrives at z = 3 mm. The rotation velocity of C IV ions is large; it reaches ~ $4 \cdot 10^6$ cm/s, which is comparable to implosion velocity of main Ar plasma. The rotation after 900 ns decreases and disappears.

At z = 5 mm, rotation is measured from ~550 ns since carbon impurities arrive later. It is interesting to note that after ~900 ns, rotation decreases but it also changes the sign, which is unexpected.

At z = 7 mm, rotation is measured from ~800 ns, with rotation sign different that at previous z positions.

The change of sign of rotation is something that needs further experimental investigation.

References

[1] N. Qi, E. W. Rosenberg, P. A. Gourdain, P. W. L. de Grouchy, B. R. Kusse, D. A. Hammer, K. S. Bell, T. A. Shelkovenko, W. M. Potter, L. Atoyan, A. D. Cahill, M. Evans, J. B. Greenly, C. L. Hoyt, S. A. Pikuz, P. C. Schrafel, E. Kroupp, A. Fisher, and Y. Maron, *Study of Gas-Puff Z-Pinches on COBRA*, Phys. Plasmas **21**, 112702 (2014).

[2] J. L. Giuliani, J. W. Thornhill, E. Kroupp, D. Osin, Y. Maron, A. Dasgupta, J. P. Apruzese, A. L. Velikovich, Y. K. Chong, A. Starobinets, V. Fisher, Y. Zarnitsky, V. Bernshtam, A. Fisher, T. A. Mehlhorn, and C. Deeney, *Effective versus Ion Thermal Temperatures in the Weizmann Ne Z-Pinch: Modeling and Stagnation Physics*, Phys. Plasmas **21**, 31209 (2014).

[3] G. Rosenzweig, E. Kroupp, T. Queller, A. Starobinets, Y. Maron, V. Tangri, J. L. Giuliani, and A. Fruchtman, *Local Measurements of the Spatial Magnetic Field Distribution in a Z-Pinch Plasma during and near Stagnation Using Polarization Spectroscopy*, Phys. Plasmas **27**, 22705 (2020).

[4] E. Kroupp, D. Osin, A. Starobinets, V. Fisher, V. Bernshtam, Y. Maron, I. Uschmann, E. Förster, A. Fisher, and C. Deeney, *Ion-Kinetic-Energy Measurements and Energy Balance in a Z-Pinch Plasma at Stagnation*, Phys. Rev. Lett. **98**, 115001 (2007).

[5] E. Kroupp, D. Osin, A. Starobinets, V. Fisher, V. Bernshtam, L. Weingarten, Y. Maron, I. Uschmann, E. Förster, A. Fisher, M. E. Cuneo, C. Deeney, and J. L.

Giuliani, *Ion Temperature and Hydrodynamic-Energy Measurements in a Z-Pinch Plasma at Stagnation*, Phys. Rev. Lett. **107**, 105001 (2011).

[6] D. Osin, E. Kroupp, A. Starobinets, G. Rosenzweig, D. Alumot, Y. Maron, A. Fisher, E. Yu, J. L. Giuliani, and C. Deeney, *Evolution of MHD Instabilities in Plasma Imploding Under Magnetic Field*, IEEE Trans. Plasma Sci. **39**, 2392 (2011).

[7] E. Stambulchik, K. Tsigutkin, and Y. Maron, *Spectroscopic Method for Measuring Plasma Magnetic Fields Having Arbitrary Distributions of Direction and Amplitude*, Phys. Rev. Lett. **98**, 225001 (2007).

[8] S. Tessarin, D. Mikitchuk, R. Doron, E. Stambulchik, E. Kroupp, Y. Maron, D. A. Hammer, V. L. Jacobs, J. F. Seely, B. V Oliver, and A. Fisher, *Beyond Zeeman Spectroscopy: Magnetic-Field Diagnostics with Stark-Dominated Line Shapes*, Phys. Plasmas **18**, 93301 (2011).

[9] D. D. Ryutov, M. S. Derzon, and M. K. Matzen, *The Physics of Fast Z Pinches*, Rev. Mod. Phys. **72**, 167 (2000).

[10] G. Rosenzweig, E. Kroupp, A. Fisher, and Y. Maron, *Measurements of the Spatial Magnetic Field Distribution in a Z-Pinch Plasma throughout the Stagnation Process*, J. Instrum. **12**, P09004 (2017).

[11] D. Mikitchuk, M. Cvejić, R. Doron, E. Kroupp, C. Stollberg, Y. Maron, A. L. Velikovich, N. D. Ouart, J. L. Giuliani, T. A. Mehlhorn, E. P. Yu, and A. Fruchtman, *Effects of a Preembedded Axial Magnetic Field on the Current Distribution in a Z-Pinch Implosion*, Phys. Rev. Lett. **122**, 45001 (2019).